Preprints of the 19th World Congress
The International Federation of Automatic Control
Cape Town, South Africa. August 24-29, 2014

Gain Scheduling H_2/H_∞ Structural Control of a Floating Wind Turbine ⋆

Yulin Si, Hamid Reza Karimi

Department of Engineering, Faculty of Engineering and Science, University of Agder, N-4898 Grimstad, Norway (e-mail: yulin.si@uia.no; hamid.r.karimi@uia.no)

Abstract: For wind turbine load mitigation, this paper proposes an active structural control deign of a hybrid mass damper installed at the tower top of a spar-type floating wind turbine. System dynamic model is established based on first principles and the polynomial curve fitting approach, while different steady-state points are derived. Then, a gain scheduling H_2/H_∞ state feedback controller is designed by solving linear matrix inequalities, which aims to reduce the loading. At last, nonlinear simulations are performed under different wind and wave conditions, and the results demonstrate that more load reduction could be achieved at the expense of more energy consumption in mass damper actuator.

Keywords: Floating wind turbine, dynamic modelling, structural control, hybrid mass damper (HMD), H_2/H_∞ control design, gain scheduling, linear matrix inequality (LMI)

1. INTRODUCTION

Floating offshore wind turbine has been a hot topic in wind energy exploration during the past few years. It provides the opportunities of cheap and clean power supply for those highly populated places near to deep offshore, such as coastal cities in the US, Spain, Japan, Korea, and Norway, see Breton and Moe (2009).

There are many engineering challenges in developing floating windmills, see Butterfield et al. (2005), among which the key difficulty lies in the additional loads caused by extra degrees of freedom (DOFs) of floating platforms. Different methods have been proposed to mitigate the fatigue and ultimate loading of tower and blades for floating wind turbines. One idea is to improve the blade pitch control strategy in order to avoid negative damping or even provide active damping of platform tilt motion, such as the works in Larsen and Hanson (2007); Namik and Stol (2010); Lackner (2013). In contrast, this work focuses on another approach, which proposes to install structural vibration control devices either in the nacelle or platform of floating wind turbines for direct load reduction. This method has been successfully used in civil engineering applications, such as vibration inhibition of buildings and bridges, see Korkmaz (2011).

In 2008, the authors in Murtagh et al. (2008) investigated the use of a tuned mass damper (TMD) placed at the tower top of a simplified wind turbine model for vibration mitigation. Following the same installation idea, Colwell et al. explored the structural responses of a fixed-bottom offshore wind turbine with a tuned liquid column damper (TLCD), see Colwell and Basu (2009). However, these discussions are only about fixed-bottom wind turbines, while their intrinsic dynamics are quite different from that of floating types. Besides, these works are not based on the cutting edge high-fidelity codes, which may not capture the comprehensive coupled nonlinear dynamics of wind turbines. Later, based on the aero-hydro-servo-elastic wind turbine numerical simulator FAST (fatigue, aerodynamics, structures, and turbulence), see Jonkman and Buhl Jr (2005), Lackner et al. implemented a new simulation tool, called FAST-SC, for passive, semi-active, and active structural control design of wind turbines, see Lackner and Rotea (2011a). The code incorporates extra DOFs of structural control devices which are installed either in wind turbine nacelle or platform (if floating) into the state-of-the-art wind turbine simulator FAST. Utilizing this code, Lackner et al. presented more realistic simulation results by installing a TMD in the nacelle of both a barge-type and a monopile supported wind turbines, see Lackner and Rotea (2011a). For more comprehensive parametric study, they also established a 3-DOF dynamic model for different types of floating wind turbines based on first principles, see Stewart and Lackner (2013), and TMD parameters are determined under different optimization methods. However, the coupling between platform surge and pitch motion was not captured in their model. This effect can be ignored for the barge model but might be a strong mode for other platforms Namik and Stol (2011); Jonkman (2010). Si et al. then improved the model by incorporating platform surge and heave modes when considering a spar-type floating wind turbine, see Si et al. (2013, 2014), but still aerodynamic load has not been considered yet, which is necessary to determine different steady states. Compared with passive design, recent research results showed that more load reduction could be achieved when introducing active structural control. In Lackner and Rotea (2011b), H_∞ multi-variable loop shaping technique was utilized for

⋆ This work has been (partially) funded by Norwegian Centre for Offshore Wind Energy (NORCOWE) under grant 193821/S60 from Research Council of Norway (RCN). NORCOWE is a consortium with partners from industry and science, hosted by Christian Michelsen Research.

active feedback structural control design of a barge-type floating wind turbine. The actuator dynamics and control-structure interaction in active control were also considered in Stewart and Lackner (2011). Nevertheless, the 3-DOF model in these works still did not include either platform surge mode or wind loads. Therefore, better modelling and control techniques are in demand to improve and verify this design.

This work will discuss the modelling and control design for load mitigation of a spar-type floating wind turbine, where a hybrid mass damper (HMD) is installed in the nacelle. Section 2 presents the modelling improvement by introducing aerodynamic thrust and approximating the nonlinearities in hydrodynamic and mooring loads. After linearization, a gain scheduling state-feedback H_2/H_∞ structural controller is designed in Section 3. Then, FAST-SC simulation results based on the proposed design is given in Section 4. Conclusions are drawn in the last section.

2. DYNAMIC MODELING

In 2009, one Norwegian company Statoil developed the world first full scale experimental floating wind turbine "Hywind". In cooperation with Statoil, Jonkman from the National Renewable Energy Laboratory (NREL) specified a detailed model for OC3-Hywind spar, which combines the data of the 5MW baseline wind turbine from NREL and the Hywind spar from Statoil, see Table 1.

Table 1. Properties of the 5MW OC3-Hywind model according to Jonkman (2010); Jonkman et al. (2009).

Item	Value
Rating	5 MW
Rotor configuration	Upwind, 3 blades
Cut-in, rated, cut-out wind speed	3 m/s, 11.4 m/s, 25 m/s
Total draft below sea water level (SWL)	120 m
Tower base above SWL	10m
Hub height above SWL	90m
Nacelle dimension (length, width, height)	14.2m, 2.3m, 3.5m
Platform diameter above taper	6.5m
Platform diameter below taper	9.4m
Rotor nacelle assembly (RNA) mass	350,000kg
Tower mass	249,718 kg
Platform mass	7,466,000 kg
Number of mooring lines	3
Depth to fairleads below SWL	70m
Baseline control in Region 3	GSPI and constant torque

The structural control idea in this work is illustrated in Fig. 1, where an HMD is installed in the nacelle of OC3-Hywind. The HMD consists of a TMD with mass M, spring and damping constants K and D, and an actuator acting force F on the mass. Since FAST-SC does not support model linearization yet, establishing the dynamic model is considered as a good option to facilitate parameter tuning and control design.

2.1 Overall Longitudinal Dynamics

Based on the D'Alembert's principle of inertial forces, the following longitudinal model can be established as follows, see Si et al. (2013).

$$\mathbf{M}(\mathbf{q})\ddot{\mathbf{q}} + \mathbf{L}(\mathbf{q}, \dot{\mathbf{q}}) = \mathbf{F}, \tag{1}$$

where

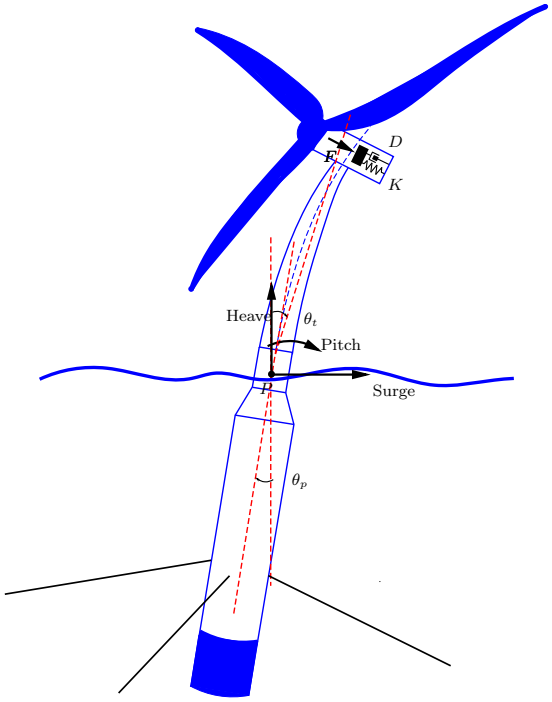

Fig. 1. Illustration of the active structural control of OC3-Hywind.

$$\mathbf{q} = \begin{bmatrix} x_{sg} \\ x_{hv} \\ \theta_p \\ x_{hmd} \\ \theta_t \end{bmatrix}, \ \mathbf{M}(\mathbf{q}) = \begin{bmatrix} M_{sg}^{sg} & 0 & I_{sg}^{p} & M_{sg}^{hmd} & 0 \\ 0 & M_{hv}^{hv} & I_{hv}^{p} & M_{hv}^{hmd} & 0 \\ M_{p}^{sg} & M_{p}^{hv} & I_{p}^{p} & M_{p}^{hmd} & 0 \\ M_{hmd}^{sg} & M_{hmd}^{hv} & I_{hmd}^{p} & M_{hmd}^{hmd} & 0 \\ M_{t}^{sg} & M_{t}^{hv} & 0 & M_{t}^{hmd} & I_{t}^{t} \end{bmatrix},$$

$$\mathbf{L}(\mathbf{q}, \dot{\mathbf{q}}) = \begin{bmatrix} F_{sg}^{hdr} + F_{sg}^{moor} + F_{sg}^{ctr} + F_{sg}^{wnd} \\ F_{hv}^{gr} + F_{hv}^{hdr} + F_{hv}^{moor} + F_{hv}^{ctr} + F_{hv}^{wnd} \\ \tau_{p}^{gr} + \tau_{p}^{hdr} + \tau_{p}^{moor} + \tau_{p}^{ctr} + \tau_{p}^{wnd} \\ F_{hmd}^{gr} + F_{hmd}^{hmd} \\ \tau_{t}^{gr} + \tau_{t}^{p} + \tau_{t}^{ctr} + \tau_{t}^{wnd} \end{bmatrix}, \mathbf{F} = \begin{bmatrix} 0 \\ 0 \\ 0 \\ F \\ 0 \end{bmatrix}.$$

In this model, $\mathbf{q}$ is the state vector, and sg, hv, p, hmd, t represent, respectively, the enabled 5 DOFs, i.e. platform surge, heave, pitch motion about P, HMD translation, and tower deflection. $\mathbf{M}(\mathbf{q})$ is the system inertial matrix, which is positive definite. M_i^j and I_i^j denote generalized mass and generalized inertial tensor for DOF i with regard to DOF j. $\mathbf{L}(\mathbf{q}, \dot{\mathbf{q}})$ represents external loads, and gr, hdr, $moor$, ctr, wnd describe, respectively, gravitational, hydro, mooring, centripetal, aerodynamic loads in forces or moments.

However, the aerodynamic load was not characterized in Si et al. (2013, 2014), where hydrodynamic and mooring loads were approximated by linear or quadratic terms around zero-displacement position. It is shown in Jonkman (2010) that there will exist strong hydrodynamic and mooring nonlinearities if the wind turbine is blown far away from its initial position, thus better representation of these loads is needed.

2.2 Hydrodynamic Loads

The nonlinearity of hydrodynamic loads mainly come from platform viscous drag, and it was approximated by linear and quadratic terms in Si et al. (2013, 2014) as shown in Fig. 2. However, in later model verification process,

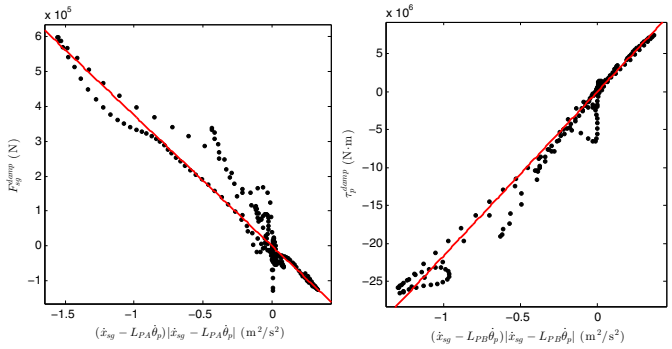

Fig. 2. Quadratic curve fitting result of drag force and its induced torque around P

it is found that this hydro damping approximation is not accurate enough to govern system dynamics. The inaccuracy is also noticeable as the fitting errors in the above figure. In this work, 3-order polynomials are used to approximate this nonlinear behaviour, which are given by

$$\begin{aligned} F_{sg}^{damp} &= a_1\dot{x}_{sg} + a_2\dot{x}_{sg}^2 + a_3\dot{x}_{sg}^3 + a_4\dot{\theta}_p, \\ \tau_p^{damp} &= b_1\dot{x}_{sg} + b_2\dot{x}_{sg}^2 + b_3\dot{x}_{sg}^3 + b_4\dot{\theta}_p. \end{aligned} \tag{2}$$

The fitting results are shown in Fig. 3, which are surprisingly much better than previous guess.

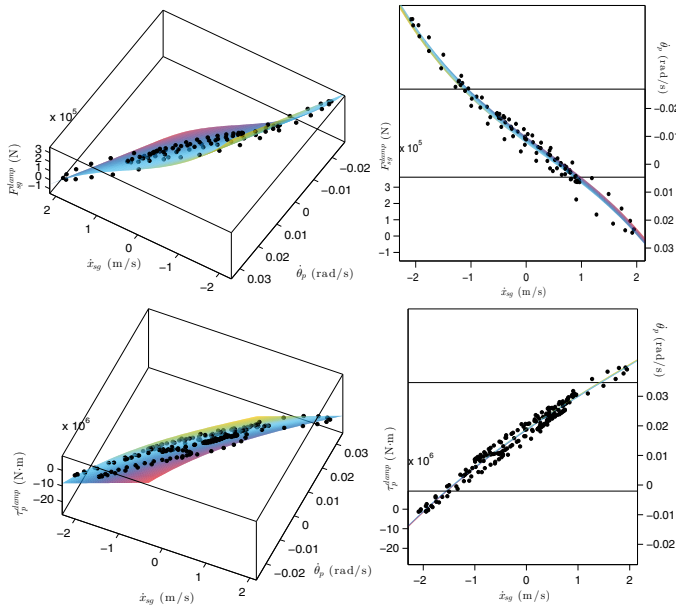

Fig. 3. Polynomial approximation result of viscous drag force and its induced torque around P.

2.3 Mooring Loads

FAST simulator uses a quasi-static model to calculate the load of an individual mooring line, which exhibits nonlinear behaviors due to both mooring dynamics and asymmetry of the three-point mooring system. The nonlinear relationship between mooring loads and platform motion are meshed in Fig. 4.

Regarding mooring system, one idea easily comes to mind that the variation of mooring loads could be determined by the surge displacement of fairleads,

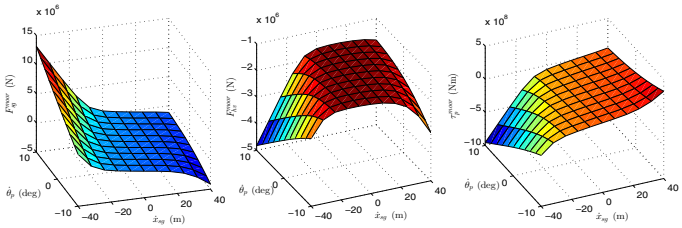

Fig. 4. Load-displacement relationships for the OC3-Hywind mooring system Jonkman (2010).

$$x_{sg}^{fair} = x_{sg} - L_{moor}\theta_p. \tag{3}$$

In order to verify this idea, mooring loads for different displacement of platform surge, heave, pitch are extracted from FAST, and the relationship between fairlead displacement in surge direction and mooring loads are demonstrated in Fig. 5. Obviously, they are almost smooth curves, thus it is possible to use polynomials to approximate this functional relationship. It needs noting that the three-line mooring system also brings asymmetry to the load-displacement relationship, so that it is more proper to use two separate polynomials in the curve fitting process. Considering fitting accuracy, the separation point is located at -20m of fairlead surge displacement. As also shown in Fig. 5, perfect curve fitting results can be achieved , and the polynomials for F_{sg}^{moor} and F_{hv}^{moor} are expressed as

$$\begin{aligned} F_{sg}^{moor} &= c_1(x_{sg}^{fair}) + c_2(x_{sg}^{fair})^2 + c_3(x_{sg}^{fair})^3, \\ F_{hv}^{moor} &= d_1(x_{hv}^{fair})^2 + d_2(x_{sg}^{fair})^3 + d_3(x_{sg}^{fair})^4. \end{aligned} \tag{4}$$

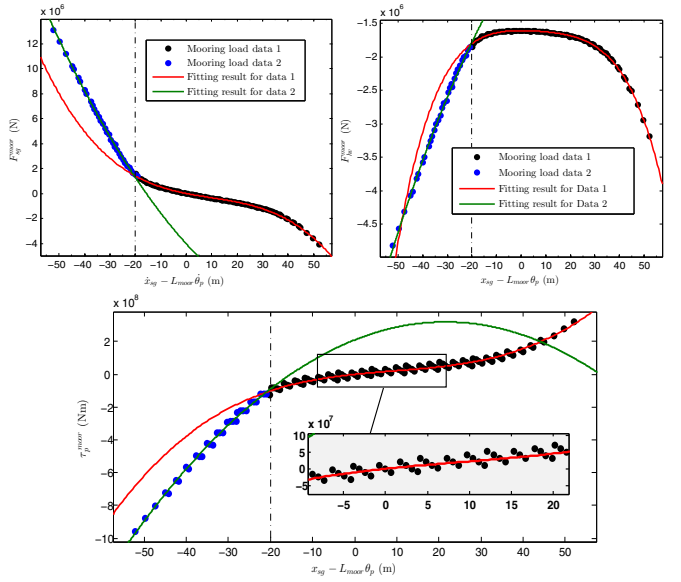

Fig. 5. Relationship approximation between mooring loads for system surge/heave/pitch modes and fairlead surge displacement.

However, when it comes to mooring torque for platform pitch motion, the assumed functional relationship is not valid, which has been amplified in Fig. 5. This is because not only fairlead surge, but also platform pitch will affect the mooring torque. Therefore, θ_p needs to be considered in the curve fitting process for τ_p^{moor}. The proposed approximation is described as

$$\tau_p^{moor} = e_1(x_{sg}^{fair}) + e_2(x_{sg}^{fair})^2 + e_3(x_{sg}^{fair})^3 + e_4\theta_p, \quad (5)$$

and the effectiveness could then be seen in Fig. 6.

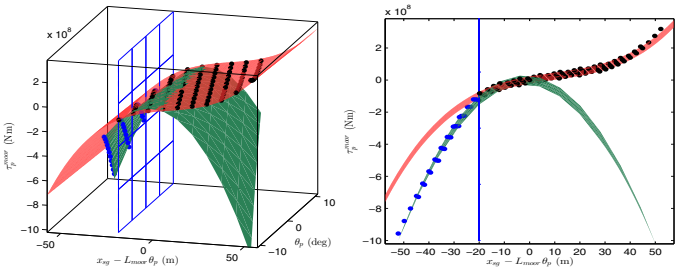

Fig. 6. Relationship among mooring torque around P, fairlead surge displacement, and platform pitch angle.

2.4 Aerodynamic Loads

According to Jonkman (2007), the dominant component of wind turbine aerodynamic loads is the aerodynamic rotor thrust T, which can be represented as the sum of a constant rotor thrust and the aerodynamic damping. After the first-order Taylor series expansion, the expression of T will be expressed as

$$T = T_0 - \left.\frac{\partial T}{\partial \theta_t}\right|_V \dot{\theta}_t, \quad (6)$$

where T_0 is the aerodynamic rotor thrust at a steady state point. V is the rotor-disk-averaged wind speed, and θ_t denotes the tower tilt angle.

It needs noting that either steady-state aerodynamic thrust T_0 or thrust sensitivity to wind speed $\frac{\partial T}{\partial \theta_t}$ depends on hub-height wind speed, rotor rotation speed, and blade pitch angle, thus listing the relationships among these factors at different steady states is necessary. Table 2 gives different steady states with varying wind speeds, where T_0 and $\left.\frac{\partial T}{\partial \theta_t}\right|_V$ need to be estimated.

2.5 Model Verification

In the verification process, generator torque and blade pitch control are both disabled, and the rotor speed and blade pitch angle are set as constant for each equilibrium point. T_0 and $\left.\frac{\partial T}{\partial \theta_t}\right|_V$ are estimated for each equilibrium point. The identification results with previous load approximation are satisfactory, e.g., the 8m/s case is shown in Fig. 7.

3. GAIN SCHEDULING H_2/H_∞ CONTROL DESIGN

3.1 Model Linearization

Based on small deviation approximation, the model around each equilibrium point can be linearized into the following state-space representation,

$$\begin{cases} \dot{x} = Ax + Bu \\ z = Cx \end{cases}, \quad (7)$$

where $x = \left[\dot{x}_{sg}, \dot{x}_{hv}, \dot{\theta}_p, \dot{x}_{hmd}, \dot{\theta}_t, x_{sg}, x_{hv}, \theta_p, x_{hmd}, \theta_t\right]^T$ is the state vector. $u = F$ is the control input, and $z = \theta_p - \theta_t$ is the controlled output.

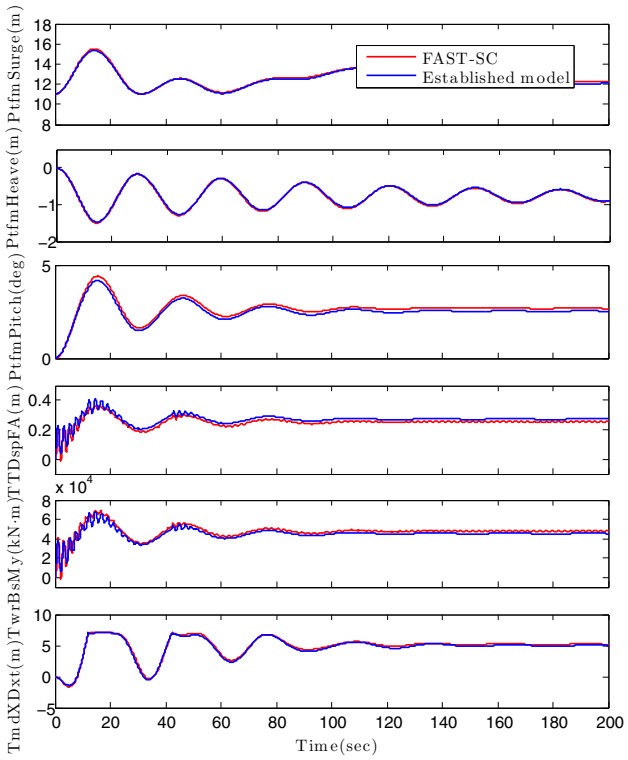

Fig. 7. Dynamic response comparison with wind load approximation.

Table 2. OC3-Hywind 5MW turbine steady-state points under different wind speeds.

V (m/s)	ω (RPM)	θ_b (°)	x_{sg} (m)	x_{hv} (m)	θ_p (°)	T_0 (10^5 N)	$\frac{\partial T}{\partial V}$ (10^6 N·s)
3.0	6.97	0.00	2.44	-0.02	0.47	0.7414	2.9428
4.0	7.18	0.00	3.90	-0.04	0.79	1.1733	3.1436
5.0	7.50	0.00	5.67	-0.07	1.15	1.6817	3.4245
6.0	7.92	0.00	7.72	-0.10	1.58	2.2563	3.8583
7.0	8.43	0.00	10.02	-0.14	2.05	2.8900	4.5637
8.0	9.07	0.00	12.67	-0.20	2.59	3.6172	5.3733
9.0	10.17	0.00	16.09	-0.29	3.28	4.5504	5.9377
10.0	11.27	0.00	19.85	-0.41	4.03	5.5921	6.5443
11.0	11.84	0.00	23.28	-0.53	4.73	6.5711	7.1261
12.0	12.10	2.96	21.31	-0.44	4.33	6.0740	8.0656
13.0	12.10	6.19	17.89	-0.35	3.66	5.1049	8.9981
14.0	12.10	8.34	16.04	-0.29	3.29	4.5911	9.5531
15.0	12.10	10.21	14.67	-0.25	3.01	4.1898	9.9529
16.0	12.10	11.84	13.60	-0.22	2.80	3.8990	10.2480
17.0	12.10	13.34	12.75	-0.20	2.64	3.6610	10.4610
18.0	12.10	14.73	12.05	-0.18	2.50	3.4804	10.4800
19.0	12.10	16.05	11.47	-0.16	2.39	3.3292	10.3800
20.0	12.10	17.34	10.95	-0.14	2.29	3.1847	10.2720
21.0	12.10	18.60	10.51	-0.12	2.20	3.0691	10.0460
22.0	12.10	19.83	10.13	-0.11	2.13	2.9717	9.7724
23.0	12.10	21.02	9.79	-0.10	2.06	2.8791	9.5400
24.0	12.10	22.19	9.49	-0.08	2.01	2.7977	9.4149
25.0	12.10	23.31	9.23	-0.07	1.96	2.7326	9.4154

3.2 H_2/H_∞ Control Design

Similar to (7), consider the linear system around a certain setpoint

$$\begin{cases} \dot{x} = Ax + Bu + B_w w \\ z = Cx \end{cases}, \quad (8)$$

where w is the aerodynamic disturbance acting on the rotor. We would like to design a state feedback controller $u = Kx$ that keeps the closed-loop system

$$\begin{cases} \dot{x} = (A + BK)x + B_w w \\ z = Cx \end{cases} \quad (9)$$

asymptotically stable and improves the dynamic performance of the closed-loop system simultaneously. More specifically, regarding performance improvement, the controller should keep the closed-loop system robust to disturbance w, i.e. the H_∞ norm of the transfer function T_{wz} in the closed-loop system does not exceed a given upper bound γ_1. More importantly, the H_2 norm of T_{wz} should be as small as possible (e.g. less than γ_2) so that the vibration energy of tower top deflection will be reduced.

Therefore, this problem is equivalent to a mixed H_2/H_∞ control design, see Scherer (1995); Doyle et al. (1994), and the design objective is to determine a desired state feedback gain K such that the closed-loop system is asymptotically stable and γ_2 is minimal for the controllers such that

$$\|T_{wz}\|_\infty < \gamma_1, \|T_{wz}\|_2 < \gamma_2.$$

The following theorem helps to convert the H_2/H_∞ control design problem into an optimization process for several linear matrix inequalities (LMIs). It is then more convenient to solve by using well developed LMI toolbox.

Theorem 1. For the closed-loop system (9), if there exists a given $\gamma_1 > 0$ and the following LMIs have an optimal solution,

$$\begin{aligned} &\min \gamma_2 \\ s.t. &\begin{bmatrix} AX+BW+(AX+BW)^T & B_w & (CX)^T \\ B_w^T & -\gamma_1 I & 0 \\ CX & 0 & -\gamma_1 I \end{bmatrix} < 0 \\ &AX+BW+(AX+BW)^T + B_w B_w^T < 0 \\ &\begin{bmatrix} -Z & CX \\ (CX)^T & -X \end{bmatrix} < 0 \\ &Trace(Z) < \gamma_2 \end{aligned} \quad (10)$$

where $X = X^T > 0$, $Z = Z^T > 0$ and W are matrices of appropriate dimensions, then the state feedback H_2/H_∞ control design is feasible, and the control law is

$$u = WX^{-1}x. \quad (11)$$

3.3 Gain Scheduling

It is possible to design a controller for each steady-state point, but controller switching will be frequent and when to switch becomes a problem. Therefore, these setpoints are categorized in 7 intervals, which are determined by rotor speed and blade pitch angle, which are possible to obtain from a wind turbine.

3.4 Low Pass Filter

The control force has to pass a second order low pass filter,

$$G(s) = \frac{\omega^2}{s^2 + 2\zeta\omega s + \omega^2},$$

which represents the actuator dynamics. Here $\omega = 10$ rad/s and ζ=0.5.

4. SIMULATION ANALYSIS

In this section, based on the control design, fully nonlinear simulations are performed in FAST-SC with all wind turbine DOFs enabled. Each test runs 630 seconds, and the output data in first 30s are not recorded, waiting for generator torque and blade pitch motion arriving normal operation state. The modified generator torque and blade pitch controller from NREL is used in the form of a dynamic link library for all tests Jonkman (2010).

In total, we consider two different simulation scenarios. The wind and wave conditions in Lackner and Rotea (2011b) are adopted as two cases in this experiment. For wind condition, the mean value of the turbulent wind is defined as 10 m/s and 18 m/s respectively. The turbulent wind file is generated by TurbSim, where Kaimal spectra and the power law exponent of 0.14 are used according to the IEC61400-3 offshore wind turbine design standard. The normal turbulence intensity is set as level B, i.e. 18% (10 m/s case) and 15%(18 m/s case). For wave condition, JONSWAP spectrum is utilized to generate the stochastic wave inputs. The significant wave height is set as 2.3 m (10 m/s case) and 3.7 m (18 m/s case), and the peak spectral period is defined as 14s. For each case, at least two sets of random variables are used to generate wind and wave data.

According to the parameter study in Si et al. (2013); Stewart and Lackner (2013), the property of the hybrid mass damper on tower top is chosen as follows, which matches first tower fore-aft vibration mode.

Table 3. Property of the hybrid mass damper in simulation.

Mass m	Spring constant K	Damping constant D
20,000 kg	120,000 N/m	16,000 N/(m/s)

Nonlinear simulation results for tower bottom load reduction can be seen in Table 4. Compared with the passive case, more load reduction can be achieved with the designed controller. One simulation comparison is illustrated in Fig. 8. $TwrBsMxt$ and $TwrBsMyt$ denote side-side and fore-aft tower base bending moment, respectively. TmdXDxt is the HMD displacement, and TmdXFext is the actuating force. However, this load reduction improvement is based on more energy consumption in HMD, and it could also be risky for instability.

Table 4. Percentage of load reduction for passive and active structural control (%)

Case	Term	Passive	Active
10m/s	DEL tower fore-aft bending	9.7	12.7
	DEL tower side-side bending	35.1	40.3
	95th tower fore-aft bending	4.1	2.57
	95th tower side-side bending	11.7	11.4
18m/s	DEL tower fore-aft bending	4.1	6.5
	DEL tower side-side bending	32.4	42.25
	95th tower fore-aft bending	0.3	0.2
	95th tower side-side bending	14.9	19.3

5. CONCLUSION

This paper dealt with a gain scheduling H_2/H_∞ active structural control deign for a hybrid mass damper installed at the tower top of the OC3-Hywind floating wind turbine. Firstly, system dynamic model was improved based on polynomial curve fitting approach, and different steady-state points were derived. Then, a gain scheduling H_2/H_∞

state feedback controller was designed by solving linear matrix inequalities, which aimed to reduce the tower bottom loads. At last, nonlinear simulations were performed under different wind and wave conditions, and the results demonstrated that more load reduction could be achieved at the expense of more energy consumption.

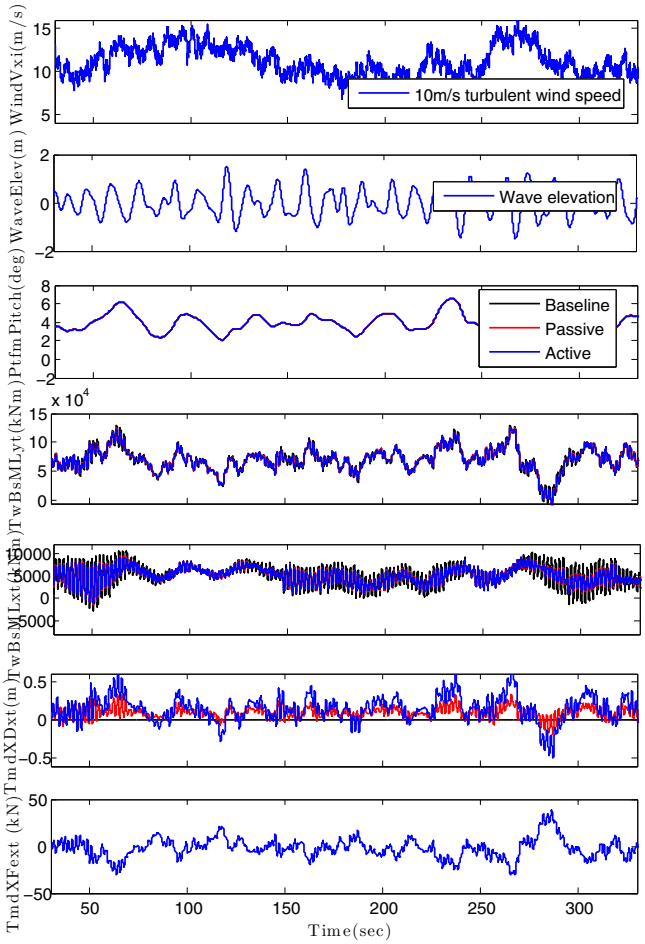

Fig. 8. Nonlinear simulation comparison under 10m/s turbulent wind and 2.3m wave.

ACKNOWLEDGEMENTS

The authors would like to give sincere thanks to Dr. Lackner in University of Massachusetts Amherst and Dr. Jonkman from National Renewable Energy Laboratory for their help on this work.

REFERENCES

Breton, S.P. and Moe, G. (2009). Status, plans and technologies for offshore wind turbines in europe and north america. *Renewable Energy*, 34(3), 646–654.

Butterfield, S., Musial, W., Jonkman, J., Sclavounos, P., and Wayman, L. (2005). Engineering challenges for floating offshore wind turbines. In *Copenhagen Offshore Wind 2005 Conference and Expedition Proceedings, 26–28 October 2005, Copenhagen, Denmark*.

Colwell, S. and Basu, B. (2009). Tuned liquid column dampers in offshore wind turbines for structural control. *Engineering Structures*, 31(2), 358–368.

Doyle, J., Zhou, K., Glover, K., and Bodenheimer, B. (1994). Multiobjective H_2/H_∞ control. *IEEE Transactions on Automatic Control*, 39(8), 1575–1587.

Jonkman, J. (2010). Definition of the floating system for phase IV of OC3. *NREL/TP-500-38060. Golden, Colorado: National Renewable Energy Laboratory*.

Jonkman, J., Butterfield, S., Musial, W., and Scott, G. (2009). Definition of a 5-mw reference wind turbine for offshore system development. Technical report, NREL/TP-500-47535. Golden, Colorado: National Renewable Energy Laboratory.

Jonkman, J. (2007). *Dynamics modeling and loads analysis of an offshore floating wind turbine*. Ph.D. thesis, Department of Aerospace Engineering Sciences, University of Colorado.

Jonkman, J. and Buhl Jr, M. (2005). Fast users guide. Technical report, NREL/EL-500-29798. Golden, Colorado: National Renewable Energy Laboratory.

Korkmaz, S. (2011). A review of active structural control: challenges for engineering informatics. *Computers & Structures*, 89, 2113–2132.

Lackner, M.A. (2013). An investigation of variable power collective pitch control for load mitigation of floating offshore wind turbines. *Wind Energy*, 16(3), 435–444.

Lackner, M.A. and Rotea, M.A. (2011a). Passive structural control of offshore wind turbines. *Wind Energy*, 14(3), 373–388.

Lackner, M.A. and Rotea, M.A. (2011b). Structural control of floating wind turbines. *Mechatronics*, 21(4), 704–719.

Larsen, T.J. and Hanson, T.D. (2007). A method to avoid negative damped low frequent tower vibrations for a floating, pitch controlled wind turbine. *Journal of Physics: Conference Series*, 75(1).

Murtagh, P.J., Ghosh, A., Basu, B., and Broderick, B.M. (2008). Passive control of wind turbine vibrations including blade/tower interaction and rotationally sampled turbulence. *Wind Energy*, 11(4), 305–317.

Namik, H. and Stol, K. (2010). Individual blade pitch control of floating offshore wind turbines. *Wind Energy*, 13(1), 74–85.

Namik, H. and Stol, K. (2011). Performance analysis of individual blade pitch control of offshore wind turbines on two floating platforms. *Mechatronics*, 21(4), 691–703.

Scherer, C.W. (1995). Multiobjective H_2/H_∞ control. *IEEE Transactions on Automatic Control*, 40(6), 1054–1062.

Si, Y., Karimi, H.R., and Gao, H. (2013). Modeling and parameter analysis of the OC3-hywind floating wind turbine with a tuned mass damper in nacelle. *Journal of Applied Mathematics*, 679071.

Si, Y., Karimi, H.R., and Gao, H. (2014). Modelling and optimization of a passive structural control design for a spar-type floating wind turbine. *Engineering Structures, to appear*.

Stewart, G. and Lackner, M. (2013). Offshore wind turbine load reduction employing optimal passive tuned mass damping systems. *IEEE Transactions on Control Systems Technology*, 21(4), 1090–1104.

Stewart, G.M. and Lackner, M.A. (2011). The effect of actuator dynamics on active structural control of offshore wind turbines. *Engineering Structures*, 33(5), 1807–1816.